Cellular Hydraulics Suggests a Poroelastic Cytoplasm Rheology

Cellular hydraulics suggests a poroelastic cytoplasm rheology

E. Moeendarbary[1,2], L. Valon[2,6], M. Fritzsche[2,3], A. R. Harris[2,3], D.A. Moulding[4], A.J. Thrasher[4], E. Stride[7], L. Mahadevan[8] and G.T. Charras[2,5]

[1]Department of Mechanical Engineering, [2]London Centre for Nanotechnology, [3]Department of Physics and Astronomy, [4]Molecular Immunology Unit, Institute of Child Health, [5]Department of Cell and Developmental Biology, University College London, London, WC1E 6JF, UK; [6]Department of Physics, Ecole Normale Superieure, Paris, France; [7]Institute of Biomedical Engineering, Department of Engineering Science, University of Oxford, Oxford OX1 3PJ, UK; [8]School of Engineering and Applied Sciences, Department of Physics, Harvard University, Cambridge, MA 02138, USA.

ABSTRACT

The cytoplasm represents the largest part of the cell by volume and hence its rheology sets the rate at which cellular shape change can occur. Recent experimental evidence suggests that cytoplasmic rheology can be described using a poroelastic formulation[1] in which the cytoplasm is considered a biphasic material constituted of a porous elastic solid meshwork (cytoskeleton, organelles, macromolecules) bathed in an interstitial fluid (cytosol). In this picture, the rate of cellular deformation is limited by the rate at which intracellular water can redistribute within the cytoplasm. Though this is a conceptually attractive model, direct supporting evidence has been lacking. Here we present such evidence and directly validate this concept to explain cellular rheology at physiologically relevant time-scales using microindentation tests in conjunction with mechanical, chemical and genetic treatments. Our results show that water redistribution through the solid phase of cytoplasm (cytoskeleton and crowders) plays a fundamental role in setting cellular rheology.

Cell mechanics | poroelasticity | viscoelasticity | microstructure

Contributions: LM, EM and GC designed the research; EM and LV performed the research with some contributions from MF and DM; EM analysed the data; EM, LV, DM, AT, and GC generated reagents; EM, LV, MF, AH, ES and LM contributed analytical tools; EM, LM, and GC wrote the paper.

One of the most striking features of eukaryotic cells is their capacity to change shape in response to environmental or intrinsic cues driven primarily by their actomyosin cytoskeleton. During gross changes in cell shape, induced either by intrinsic switches in cell behaviour (e.g. cell rounding, cytokinesis, cell spreading, or cell movement) or by extrinsic stress application during normal organ function, the maximal rate at which shape change can occur is dictated by the rate at which the cytoplasm can be deformed because it forms the largest part of the cell by volume. Furthermore, it is widely recognised that cells detect, react, and adapt to external mechanical stresses. However, in the absence of an in depth understanding of cell rheology, the transduction of external stresses into intracellular mechanical changes is poorly understood making the identification of the physical parameters that are detected biochemically purely speculative[2].

Living cells are complex materials displaying a high degree of structural hierarchy and heterogeneity coupled with active biochemical processes that constantly remodel their internal structure. Therefore, perhaps unsurprisingly, they display an astonishing variety of rheological behaviours depending on amplitude, frequency and spatial location of loading[2,3]. Over the years, a rich phenomenology of rheological behaviours has been uncovered in cells such as scale-free power law rheology, strain stiffening, anomalous diffusion, and rejuvenation (reviewed in [2-6]). Several theoretical models explain these observed behaviours but finding a unifying theory has been difficult because different microrheological measurement techniques excite different modes of relaxation[2]. These rheological models range from those that treat the cytoplasm as a single phase material whose rheology is described using networks of spring and dashpots[7,8], to the sophisticated soft glassy rheology (SGR) models that describe cells as being akin to soft glassy materials close to a glass transition[9,10]; in either case, the underlying geometrical and biophysical phenomena remain poorly defined[2,5,6]. Furthermore, none of the models proposed account for dilatational changes in the multiphase material that is the cytoplasm. Yet, these volumetric deformations are ubiquitous in the context of phenomena such as blebbing, cell oscillations or cell movement[1,11], and in gels of purified cytoskeletal proteins[12] whose macroscopic rheological properties depend on the gel structural parameters and its interaction with an interstitial fluid[13-15]. Any unified theoretical framework that aims to capture the rheological behaviours of cells and link these to cellular structural and biological parameters must account for both the shear and dilatational effects seen in cell mechanics as well as account for the role of crowding and active processes in cells.

The flow of water plays a critical part in such processes. Recent experiments suggest that pressure equilibrates slowly within cells (~10s)[1,16,17] giving rise to intracellular flows of cytosol[11,18] that cells may exploit to create lamellipodial protrusions[11] or blebs[1,19] for locomotion[20]. Furthermore, the resistance to water flow through the soft porous structure serves to slow motion in a simple and ubiquitous way that does not depend on the details of structural viscous dissipation in the cytoplasmic network. Based on these observations, a coarse-grained biphasic description of the cytoplasm as a porous elastic solid meshwork bathed in an interstitial fluid (e.g. poroelasticity[21] or the two-fluid model[22]) has been proposed as a minimal framework for capturing the essence of cytoplasmic rheology[1,17,23]. In the framework of poroelasticity, coarse graining of the physical parameters dictating cellular rheology accounts for the effects of interstitial fluid and related volume changes, macromolecular crowding and a cytoskeletal network[1,17,24], consistent with the rheological properties of the cell on the time-scales needed for redistribution of intracellular fluids in response to localised deformation. The response of cells to deformation then depends only on the poroelastic diffusion constant D_p, with larger values corresponding to more rapid stress relaxations. This single parameter scales as $D_p \sim E\,\xi^2/\mu$ with E the drained elastic modulus of the solid matrix, ξ the radius of pores in the solid matrix, and μ the viscosity of the cytosol (see supplementary information), allowing changes in cellular rheology to be predicted in response to changes in E, ξ, and μ.

Here, we probe the contribution of intracellular water redistribution to cellular rheology at time-scales relevant to cell physiology (up to 10s) and examined the relative importance of crowding and the cytoskeleton in determining cell rheology. To confirm the generality of our findings across cell types,

our experiments examined HT1080 fibrosarcoma, HeLa cervical cancer cells, and MDCK epithelial cells.

RESULTS

Cellular force-relaxation at short time-scales is poroelastic. First, we established the experimental conditions under which water redistribution within the cytoplasm might contribute to force-relaxation. In our experiments (Fig. 1A), following rapid indentation with an AFM cantilever (3.5-6nN applied during a rise time t_r~35ms resulting in δ~1µm cellular indentation), force decreased by ~35% whereas indentation depth only increased by less than ~5%, showing that our experiments measure force-relaxation under approximately constant applied strain (Fig. 1B,C). Relaxation in poroelastic materials is due to water movement out of the porous matrix in the compressed region. The time-scale for water movement is $t_p \sim L^2/D_p$ (L is the length-scale associated with indentation[25]: $L \sim \sqrt{R\delta}$ with R the radius of the indenter) and therefore poroelastic relaxation contributes significantly if the rate of force application is faster than the rate of water efflux: $t_r << t_p$. Previous experiments estimated D_p~1-100 µm^2.s^{-1} in cells[1,17] yielding a characteristic poroelastic time of t_p~0.1-10s, far longer than t_r. Hence, if intracellular water redistribution is important for cell rheology, force-relaxations curves should display characteristic poroelastic signatures for times up to t_p~0.1-10s.

Population averaged force-relaxation curves showed similar trends for both HeLa and MDCK cells with a rapid decay in the first 0.5s followed by slower decay afterwards (Fig. 1D-I). In Fig. 1D-II, we see that force-relaxation clearly displayed two separate regimes: a plateau lasting ~0.1-0.2s followed by a transition to a linear regime (Fig. 1D-II). Hence, at short time-scales, cellular force-relaxation does not follow simple power laws. Comparison with force-relaxation curves acquired on physical hydrogels[25-27], which display a plateau at short time-scales followed by a transition to a second plateau at longer time-scales (Fig. S3A-B), suggests that the initial plateau observed in cellular force-relaxation may correspond to poroelastic behaviour. Indeed poroelastic models fitted the force-relaxation data well for short times (<0.5s); whereas power law models were applicable for times longer than ~0.1-0.2s (Fig. 1D-II). Finally, when force-relaxation curves acquired for different indentation depths on cells were renormalized for force and rescaled with a time-scale dependent on indentation depth, all experimental curves collapsed onto a single master curve for short time-scales, confirming that the initial dynamics of cellular force-relaxation are due to intracellular water flow (Fig. S1-3, supplementary results). Together, these data suggested that for time-scales shorter than ~0.5s, intracellular water redistribution contributed strongly to force-relaxation, consistent with the ~0.1s time-scale measured for intracellular water flows in the cytoplasm of HeLa cells[28].

To provide baseline behaviour for perturbation experiments, we measured the elastic and poroelastic properties of MDCK, HeLa, and HT1080 cells by fitting force-indentation and force-relaxation curves with Hertzian and poroelastic models, respectively. Measurement of average cell thickness suggested that for time-scales shorter than 0.5s, cells could be considered semi-infinite and forces relaxed according to a single exponential relationship with $F(t) \sim e^{-D_p t/L^2}$ (Supplementary results, Fig. S10). In our experimental conditions (3.5-6nN force resulting in indentation depths less than 25% of cell height, Fig. S4C-D), force-relaxation with an average amplitude of 40% was observed with 80% of total relaxation occurring in ~0.5s (Fig. 1B, 1D). Analysis of the indentation curves yielded an elastic modulus of E=0.9±0.4 kPa for HeLa cells (N=189 curves on n=25 cells), E=0.4±0.2 kPa for HT1080 cells (N=161 curves on n=27 cells), and E=0.4±0.1 kPa for MDCK cells (n=20 cells). Poroelastic models fitted experimental force-relaxation curves well (on average r^2=0.95, black line, Fig. 1B-II) and yielded a poroelastic diffusion constant of D_p=41±11 µm^2.s^{-1} for HeLa cells, D_p=40±10 µm^2.s^{-1} for HT1080 cells, and D_p=61±10 µm^2.s^{-1} for MDCK cells.

Poroelasticity can predict changes in cell rheology associated with volume changes. We examined the ability of the simple scaling law $D_p \sim E\,\xi^2/\mu$ to qualitatively predict changes in D_p resulting from changes in pore size due to cell volume change, which should not affect cytoskeletal organisation or

integrity but should alter cytoplasmic pore size. To change cell volume, we exposed HeLa and MDCK cells to hyperosmotic media to decrease cell volume and hypoosmotic media to increase cell volume and measured concomitant changes in D_p.

First, we ascertained that osmotically-induced volume changes persisted long enough for experimental measurements to be effected and that control cells retained a constant volume over this duration (Fig. 2A). To ensure a stable volume increase in hypoosmotic conditions, we treated cells with regulatory volume decrease inhibitors[29] and measured a stable increase of 22±2% in cell volume after hypoosmotic treatment (Fig. 2A). Conversely, upon addition of 110 mM sucrose, cell volume decreased by 21±6% (Fig. 2A) and upon addition of PEG-400 (30% volumetric concentration), cell volume decreased drastically by 54±3% (Fig. 2A, Fig. S1E). Similar results were obtained for both cell types.

Next, we asked if changes in cell volume resulted in changes in poroelastic diffusion constant in both cell types. Consistent with results by others[30], our experiments revealed that cells relaxed less rapidly and became stiffer with decreasing fluid fraction. Increases in cell volume resulted in a significant increase in poroelastic diffusion constant D_p and a significant decrease in cellular elasticity E (Fig. 2B, C). In contrast, decrease in cell volume decreased the diffusion constant and increased elasticity (Fig. 2B, C). We verified that cytoskeletal organisation was not perturbed by changes in cell volume (Fig. S5 for actin), suggesting that change in pore size alone was responsible for the observed changes in D_p and E. Because the exact relationship between hydraulic pore size ξ and cell volume is unknown, we plotted D_p and E as a function of the change in the volumetric pore size $\psi \sim (V/V_o)^{1/3}$. For both MDCK and HeLa cells, D_p scaled with ψ and the cellular elasticity E scaled inversely with ψ (Fig. 2D). In summary, increase in cell volume increased the poroelastic diffusion constant and decrease in cell volume decreased D_p, consistent with our simple scaling law.

Changes in cell volume result in changes in cytoplasmic pore size. Having shown that changes in cell volume result in changes in poroelastic diffusion constant without affecting cytoskeletal structure, we tried to directly detect changes in pore size. To do this, we microinjected PEG-passivated quantum dots (~14nm hydrodynamic radius with the passivation layer[31]) into cells and examined their mobility. Under isoosmotic condition, quantum dots rapidly diffused throughout the cell; however, upon addition of PEG-400, they became immobile (supplementary video 1, Fig. 3A, n=7 cells examined). Hence, cytoplasmic pore size decreased in response to cell volume decrease trapping quantum dots in the cytoplasmic solid fraction and immobilising them (Fig. 3D-II). This suggested that the isoosmotic pore radius ξ was larger than 14nm, consistent with our estimates from poroelasticity (Supplementary results). Next, we verified that under hyperosmotic conditions cells retained a fluid fraction by monitoring recovery after photobleaching of a small fluorescein analog (CMFDA, hydrodynamic radius R_h~0.9nm [32]). In isoosmotic conditions, CMFDA recovered rapidly after photobleaching (black line, Fig. 3B, supplementary table S1). In the presence of PEG-400, CMFDA fluorescence still recovered, indicating the presence of a fluid-phase, but recovery slowed three-fold, consistent with [33] (grey line, Fig. 3B). The measured decrease in translational diffusion suggested a reduction in the cytoplasmic pore size with dehydration. Indeed, translational diffusion is related to the solid fraction Φ via the relation $D_T/D_{T\infty} \sim exp(-\Phi)$ with $D_{T\infty}$ the translational diffusion constant of the molecule in a dilute isotropic solution[34]. Assuming that the fluid is contained in N pores of equal radius ξ, the solid fraction is $\Phi \sim V_s/(V_s+N\xi^3)$ with V_s the volume of the solid fraction, a constant. $D_T/D_{T\infty}$ is therefore a monotonic increasing function of ξ. To examine the effect of volume increase on pore size, we examined the fluorescence recovery after photobleaching of a cytoplasmic GFP decamer (EGFP-10x, R_h~7.5nm). Increases in cell volume resulted in a significant ~2-fold increase in D_T ($p<0.01$, Fig. 3C, supplementary table S1), suggesting that pore size did increase. Together, our experiments show that changes in cell volume modulate cytoplasmic pore size ξ consistent with estimates from AFM measurements (Fig. S6A-B).

Poroelastic properties are influenced by the integrity of the cytoskeleton. Cytoskeletal organisation strongly influences cellular elasticity E[35], and is also likely to affect the cytoplasmic pore size ξ (Fig.

S7A-C). As both factors play antagonistic roles in setting D_p, we examined the effect of cytoskeletal perturbations.

Treatment of cells with 750 nM latrunculin, a drug that depolymerises the actin cytoskeleton, resulted in a significant decrease in the cellular elastic modulus (Fig. 4B, consistent with [35]), a ~two-fold increase in the poroelastic diffusion coefficient (Fig. 4A), and a significant increase in the lumped pore size (Fig. S6E). Depolymerisation of microtubules by treatment with 5 μM nocodazole had no significant effect (Fig. S6C-E). Stabilisation of microtubules with 350 nM taxol resulted in a small (-16%) but significant decrease in elasticity but did not alter D_p (Fig. S6C-E).

In light of the dramatic effect of F-actin depolymerisation on D_p and ξ, we attempted to decrease the pore size by expressing a constitutively active mutant of WASp (WASp I294T, CA-WASp) that results in excessive polymerization of F-actin in the cytoplasm through ectopic activation of the arp2/3 complex, an F-actin nucleator (Fig. 4C, [36]). Increased cytoplasmic F-actin due to CA-WASp resulted in a significant decrease in the poroelastic diffusion coefficient (-43%, $p<0.01$, Fig. 4A), a significant increase in cellular elasticity (+33%, $p<0.01$, Fig. 4B), and a significant decrease in the lumped pore size (-38%, $p<0.01$, Supplementary Fig. S6E). Similar results were also obtained for HT1080 cells (-49% for D_p, +68% for E and -38% for lumped pore size, $p<0.01$). Then, we attempted to change cell rheology without affecting intracellular F-actin concentration by perturbing crosslinking or contractility. To perturb crosslinking, we overexpressed a deletion mutant of α-actinin (ΔABD-α-actinin) that lacks an actin-binding domain but can still dimerize with endogenous protein[37], reasoning that this should either increase the F-actin gel entanglement length λ or reduce the average diameter of F-actin bundles b (Fig. 3D-I). Overexpression of ΔABD-α-actinin led to a significant decrease in E but no change in D_p or ξ (Fig. 4A-B, Fig. S6E). Perturbation of contractility with the myosin II ATPase inhibitor blebbistatin (100 μM) lead to a 50% increase in D_p, a 70% decrease in E, and a significant increase in lumped pore size (Fig. 4A-B, Fig. S6E). To determine if ectopic polymerisation of microtubules had similar effects to CA-WASp, we overexpressed γ-tubulin, a microtubule nucleator[38], but found that this had no effect on cellular elasticity, poroelastic diffusion constant, or lumped pore size (Fig. S6C-E). Finally, expression of a dominant keratin mutant (Keratin 14 R125C,[39]) that causes aggregation of the cellular keratin intermediate filament network had no effect on E, D_p, or lumped pore size (Fig. S6C-E, S7C-D).

Discussion

We have shown that water redistribution plays a significant role in cellular responses to mechanical stresses at short time-scales and that the effect of osmotic and cytoskeletal perturbations on cellular rheology can be understood in the framework of poroelasticity through a simple scaling law $D_p \sim E\,\xi^2/\mu$. Force-relaxation induced by fast localised indentation by AFM contained two regimes: at short time-scales, relaxation was poroelastic; while at longer time-scales, it exhibited a power law behaviour. We tested the dependence of D_p on the hydraulic pore size ξ by modulating cell volume and showed that D_p scaled proportionally to volume change, consistent with a poroelastic scaling law. Changes in cell volume did not affect cytoskeletal organisation but did modulate pore size. Experiments monitoring the mobility of microinjected quantum dots suggested that ξ was ~14nm consistent with estimates based on measured values for D_p and E (Supplementary results). We also confirmed that cellular elasticity scaled inversely to volume change as shown experimentally[30,40] and theoretically[14] for F-actin gels and cells. However, the exact relationship between the poroelastic diffusion constant D_p and the hydraulic pore size ξ could not be tested experimentally because the relationship between volumetric change and change in ξ is unknown due to the complex nature of the solid phase of the cytoplasm (composed of the cytoskeletal gel, organelles, and macromolecules, Fig. 3D-I, [41]). Taken together our results show that, for time-scales up to ~0.5s, the dynamics of cellular force-relaxation is consistent with a poroelastic behaviour for cells and that changes in cellular volume resulted in changes in D_p due to changes in ξ.

Cell mechanical studies over the years have revealed a rich phenomenological landscape of rheological behaviours that are dependent upon probe geometry, loading protocol and loading frequency[2-6], though the biological origin of many of these regimes remains to be fully explored. Spurred by recent reports

implicating intracellular water flows in the creation of cellular protrusions[1,11,18], we have examined the role of intracellular water redistribution in cellular rheology. Our experimental measurements indicated that intracellular fluid flows occurred for deformations applied with a rise time t_r shorter than the poroelastic time $t_p \sim L^2/D_p$ (~0.2s in our conditions), consistent with the time-scales of intracellular water flows observed in HeLa S3 cells[28]. It may appear surprising that poroelastic effects have not been considered previously and we envisage several reasons for this. First, most studies to date have investigated cellular shear rheology using techniques such as magnetic twisting cytometry [4,9,10] or bead tracking microrheology[42], which only account for isochoric deformations and thus cannot be used to study dilatational rheology where volumetric deformations, such as those induced in our experiments, arise. Second, the time-scale of intracellular water flows is highly dependent on the volume of the induced deformation. Therefore, to observe poroelastic effects experimentally, large volumetric deformations must be induced and the cellular responses must be sampled at high rate (2000 Hz in our experiments). Thus, although clues to poroelastic behaviours exist in previous experiments examining whole-cell deformation with optical stretchers which reported a short time-scale regime that could not be fit by power laws[43] and previous AFM force-relaxation experiments have reported the existence of a fast exponential decay occurring at short time scales[44,45] they were not systematically examined. Third, previous work[13] has shown that, in oscillatory experiments, for loading frequencies $f_p >> E\xi^2/(\mu L^2)$ (~5 Hz in our experimental conditions), the fluid will not move relative to the mesh and therefore that inertial and structural viscous effects from the mesh are sufficient to describe the system. Hence, intracellular water flows participate in cell rheology for loadings applied with rise times t_r shorter than t_p and repeated with frequencies lower than f_p. Such a loading regime is particularly relevant for tissues of the cardiovascular and respiratory systems where the constituent cells are routinely exposed to large strains applied at high strain rates and repeated at low frequencies (e.g. 10% strain applied at ~50%.s^{-1} repeated at up to 4 Hz for arterial walls[46], 70% strain applied at up to 900%.s^{-1} repeated at up to 4 Hz in the myocardial wall[47], and 20% strain applied at >20%.s^{-1} repeated at ~1 Hz for lung alveola[48]). Over the time-scales of our experiments (~5s), other factors such as turnover of cytoskeletal fibres and cytoskeletal network rearrangements due to crosslinker exchange or myosin contractility might also in principle influence cell rheology. In our cells, F-actin, the main cytoskeletal determinant of cellular rheology (Fig. 4 and [49,50]), turned over with a half-time of ~11s (Fig. S7C), crosslinkers turned over in ~20s[51], and myosin inhibition led to faster force-relaxation. Hence, active biological remodelling cannot account for the dissipative effects observed in our force-relaxation experiments. Taken together, the time-scale of force-relaxation, the functional form of force-relaxation, and the qualitative agreement between the theoretical scaling of D_p with experimental changes to E and ξ support our hypothesis that water redistribution is the principal source of dissipation at short time-scales contributing ~50% of total relaxation in ~0.2 s in our experiments. At time-scales short compared to 1s, force-relaxation decays exponentially in poroelastic models as it does in simple Maxwell models of the cytoplasm (Supplementary Results), but with the important difference that the Maxwell model makes no distinction between shear and dilatation, and has no microstructural basis in terms of the two phase picture of a fluid bathed network. However, in the context of observations past and present, this does suggest the following relationship for a length-scale dependent effective cellular viscosity η

$$\eta \sim \mu\left(\frac{L}{\xi}\right)^2$$

with L a characteristic length-scale and μ the viscosity of cytosol. Given the dependence of η on the ratio of a mesoscopic length-scale to a microscopic length-scale in the system may explain the large spread in reported measurements of cytoplasmic viscosities [2,7].

To gain an understanding of how widespread poroelastic effects are in the rheology of isolated cells and cells within tissues, one can compute the poroelastic Péclet number $\mathrm{Pe}=(VL)/D_p$, with V a characteristic velocity (due to active movement, external loading, etc). For Pe >> 1, poroelastic effects dominate the viscoelastic response of the cytoplasm to shape change due to externally applied loading or intrinsic cellular forces. In isolated cells, poroelastic effects have been implicated in the formation of protrusions such as lamellipodia or blebs[1]. For these, the rate of protrusion growth can be chosen as a characteristic

velocity. In rapidly moving cells, forward-directed intracellular water flows[11,18] resulting from pressure gradients due to myosin contraction of the cell rear have been proposed to participate in lamellipodial protrusion[11]. Assuming a representative lamellipodium length of L~10 μm and protrusion velocities of V~0.3 μm.s^{-1}, poroelastic effects will play an important role if $D_p \leq 3$ μm^2.s^{-1}, lower than measured in the cytoplasm but consistent with the far higher F-actin density observed in electron micrographs of the lamellipodium[20]. Furthermore, cells can also migrate using blebbing motility[52] where large quasi-spherical blebs (L~10μm) arise at the cell front with protrusion rates of V~1 μm.s^{-1} giving an estimate of D_p~10 μm^2.s^{-1} (comparable to the values reported here) to obtain Pe≥1. During normal physiological function, cells within tissues of the respiratory and cardiovascular systems are subjected to strains ε>20% applied at strain rates ε_t>20%.s^{-1}. As a first approximation, we assume that these cells, with a representative length L_{cell}, undergo a length change $L \sim \varepsilon L_{cell}$ applied with a characteristic velocity $V \sim L_{cell}\varepsilon_t$. For cells within the lung alveola[48], L_{cell}~30 μm, ε~20%, ε_t~20%.s^{-1} and assuming D_p~10 μm^2.s^{-1} (based on our measurements), we find Pe~3. Hence, these simple estimates of Pe suggest that water redistribution participates in setting the rheology of cells within tissues under normal physiological conditions.

Although the cytoskeleton plays a fundamental role in modulating cellular elasticity and rheology, our studies show that microtubules and keratin intermediate filaments do not play a significant role in setting cellular rheological properties (Fig. S6C-E). In contrast, both the poroelastic diffusion constant and elasticity strongly depended on actomyosin (Fig. 4). Our experiments qualitatively illustrated the relative importance of ξ and E in determining D_p. Depolymerising the F-actin cytoskeleton decreased E and increased pore size resulting in an overall increase in D_p. Conversely, when actin was ectopically polymerised in the cytoplasm by arp2/3 activation by CA-WASp (Fig. 4), E increased and the pore size decreased resulting in a decrease in D_p. For both perturbations, changes in pore size ξ dominated over changes in cellular elasticity in setting D_p. For dense crosslinked F-actin gels, theoretical relationships between the entanglement length λ and the elasticity E suggest that $E \sim \kappa^2/(k_B T \lambda^5)$ with κ the bending rigidity of the average F-actin bundle of diameter b, k_B the Boltzmann constant, and T the temperature[14] (Fig. 3D-I). If the hydraulic pore size ξ and the cytoskeletal entanglement length λ were identical, D_p would scale as $D_p \sim \kappa^2/(\mu k_B T \lambda^3)$ implying that changes in elastic modulus would dominate over changes in pore size, in direct contradiction with our results. Hence, ξ and λ are different and ξ may be influenced both by the cytoskeleton and macromolecular crowding[41] (Fig. 3D-I). To decouple changes in elasticity from gross changes in intracellular F-actin concentration, we decreased E by reducing F-actin crosslinking through overexpression of a mutant α-actinin[37] that can either increase the entanglement length λ or decrease the bending rigidity κ of F-actin bundles by diminishing their average diameter b (Fig. 3D-I). Overexpression of mutant α-actinin led to a decrease in E but no detectable change in D_p or ξ confirming that pore size dominates over elasticity in determining cell rheology. Finally, myosin inhibition led to an increase in D_p, a decrease in E, and an increase in ξ, indicating that myosin contractility participates in setting rheology through application of pre-stress to the cellular F-actin mesh[15], something that results directly or indirectly in a reduction in pore size[15,53]. Taken together, these results show that F-actin plays a fundamental role in modulating cellular rheology but further work will be necessary to understand the relationship between hydraulic pore size ξ, cytoskeletal entanglement length λ, crosslinking, and contractility in living cells.

Though the poroelastic framework can mechanistically describe cell rheology at short-time scales and predict changes of D_p in response to changes in microstructural and constitutive parameters, the minimal formulation provided here does not yet provide a complete framework for explaining the rich phenomenology of rheological behaviours observed over a wide ranges of time scales. However, building on the poroelastic framework's ability to link cell rheology to microstructural and constitutive parameters, it may be possible to extend its domain of applicability by including additional molecular and structural detail such as a more complex solid meshwork with the characteristics of a crosslinked F-actin gel[14] with continuous turnover and protein unfolding[54,55], or considering the effects of molecular crowding on the movement of interstitial fluid. Indeed, further intuition for the complexity and variety of length scales involved in setting cellular rheology (Fig. 3D-I) can be gained by

recognising that the effective viscosity μ felt by a particle diffusing in the cytosol will depend on its size (Fig. 3, Fig. S5 and [56,57]). Within the cellular fluid fraction, there exists a wide distribution of particle sizes with a lower limit on the radius set by the radius of water molecules. Whereas measuring the poroelastic diffusion constant D_p remains challenging, the diffusivity D_m of any given particle can be measured accurately in cells. For a molecule of radius a, the Stokes-Einstein relationship gives $D_m=k_BT/(6\pi\mu a)$ or $\mu(a)=k_BT/(6\pi D_m a)$. Any interaction between the molecule and its environment (e.g. reaction with other molecules, crowding and hydrodynamic interactions[58], size-exclusion[57]) will result in a deviation of the experimentally determined D_m from this relationship. Using the previous relationship for elasticity of gels and recalling that the bending rigidity of filaments scales as $\kappa \sim E_{polymer} b^4$ (with b the average diameter of a filament –or bundle of filaments-, and $E_{polymer}$ the elasticity of the polymeric material[59]), we obtain the relationship

$$D_p \sim \left(\frac{\xi^2 a E_{polymer}^2 b^8}{(k_B T)^2 \lambda^5}\right) D_m$$

in which four different length-scales contribute to setting cellular rheology. We see that the average filament bundle diameter b, the size of the largest particles in the cytosol a (and indeed the particle size distribution in the cytosol), the entanglement length λ, and the hydraulic pore size ξ together conspire to determine the geometric, transport, and rheological complexity of the cell (Fig. 3D-I). Since all these parameters can be dynamically controlled by the cell, it is perhaps not surprising that a rich range of rheologies has been experimentally observed in cells[2-12].

METHODS

Cell culture. Details on cell culture, drug treatments, and genetic treatments are provided in the supplementary information.

Atomic force microscopy measurements. During AFM experiments, measurements were acquired in several locations in the cytoplasm avoiding the nucleus. To maximize the amplitude of stress relaxation, the cantilever tip was brought into contact with the cells using a fast approach speed ($V_{approach}$ ~ 10-30 $\mu m.s^{-1}$) until reaching a target force set to achieve an indentation depth $\delta \sim 1\mu m$ (Fig. 1A-I, 1A-II, 1B). Force was applied onto the cells in less than 35-100 ms, short compared to the experimentally observed relaxation time. Upon reaching the target force F_M the piezoelectric ceramic length was kept at a constant length and the force-relaxation curves were acquired at constant Z_M sampling at 2000 Hz (Fig. 1A-III, A-IV). After 10s, the AFM tip was retracted.

Measurement of the poroelastic diffusion coefficient. A brief description of the governing equations of linear isotropic poroelasticity and the relationship between the poroelastic diffusion constant D_p, the elastic modulus E, and hydraulic permeability k are given in supplementary information. We analysed our experiments as force-relaxation in response to a step displacement of the cell surface. No closed form analytical solution for indentation of a poroelastic infinite half space by a spherical indentor exists. However, an approximate solution obtained by Finite-Element (FE) simulations gives[25]:

$$\frac{F(t)-F_f}{F_i-F_f} = 0.491\,\mathrm{e}^{-0.908\sqrt{\tau}} + 0.509\,\mathrm{e}^{-1.679\tau}, \qquad (1)$$

where $\tau=D_p t/R\delta$ is the characteristic poroelastic time required for force to relax from F_i to F_f. Cells have a limited thickness h and therefore the infinite half-plane approximation is only valid at time-scales shorter than the time needed for fluid diffusion through the cell thickness: $t_{hp} \sim h^2/D_p$. In our experiments on HeLa cells, we measured h~5 μm and D_p~40 $\mu m^2.s^{-1}$ setting a time-scale t_{hp}~0.6s. We confirmed numerically that for times shorter than ~0.5 s, approximating the cell to a half-plane gave errors of less than 20% (Supplementary results, Fig. S10). For short time-scales, both terms in equation (1) are comparable and hence as a first approximation, the relaxation scales as $\sim e^{-\tau}$. Equation (1) was utilized to fit our experimental relaxation data, with D_p as single fitting parameter and we fitted only the first 0.5 s of relaxation curves to consider only the maximal amplitude of poroelastic relaxation and minimise errors arising from finite cell thickness.

Acknowledgements
EM is in receipt of a Dorothy Hodgkins Postgraduate Award (DHPA) from the Engineering and Physical Sciences Research Council. LM thanks the MacArthur Foundation for support. GTC is in receipt of a Royal Society University Research Fellowship. GTC, DM and AT are funded by Wellcome Trust grant (WT092825). AT and DM are funded by Wellcome Trust grant (WT090233). AT is funded by The Great Ormond Street Children's Charity. The authors wish to acknowledge the UCL Comprehensive Biomedical Research Centre for generous funding of microscopy equipment. We also gratefully acknowledge support of Prof. N. Ladommatos and Dr. W. Suen from Department of Mechanical Engineering at UCL.

REFERENCES

1 Charras, G. T., Yarrow, J. C., Horton, M. A., Mahadevan, L. & Mitchison, T. J. Non-equilibration of hydrostatic pressure in blebbing cells. *Nature* **435**, 365-369 (2005).
2 Hoffman, B. D. & Crocker, J. C. Cell mechanics: dissecting the physical responses of cells to force. *Annual review of biomedical engineering* **11**, 259-288 (2009).
3 Fletcher, D. A. & Geissler, P. L. Active biological materials. *Annual review of physical chemistry* **60**, 469-486 (2009).
4 Trepat, X., Lenormand, G. & Fredberg, J. J. Universality in cell mechanics. *Soft Matter* **4**, 1750-1759 (2008).
5 Chen, D. T. N., Wen, Q., Janmey, P. A., Crocker, J. C. & Yodh, A. G. Rheology of soft materials. *Condensed Matter Physics* **1** (2010).
6 Kollmannsberger, P. & Fabry, B. Linear and nonlinear rheology of living cells. *Annual Review of Materials Research* **41**, 75-97 (2011).
7 Bausch, A. R., Möller, W. & Sackmann, E. Measurement of local viscoelasticity and forces in living cells by magnetic tweezers. *Biophysical journal* **76**, 573-579 (1999).
8 Alcaraz, J. *et al.* Microrheology of human lung epithelial cells measured by atomic force microscopy. *Biophysical journal* **84**, 2071-2079 (2003).
9 Fabry, B. *et al.* Scaling the microrheology of living cells. *Physical review letters* **87**, 148102 (2001).
10 Deng, L. *et al.* Fast and slow dynamics of the cytoskeleton. *Nature materials* **5**, 636-640 (2006).
11 Keren, K., Yam, P. T., Kinkhabwala, A., Mogilner, A. & Theriot, J. A. Intracellular fluid flow in rapidly moving cells. *Nature cell biology* **11**, 1219-1224 (2009).
12 Bausch, A. R. & Kroy, K. A bottom-up approach to cell mechanics. *Nature Physics* **2**, 231-238 (2006).
13 Gittes, F., Schnurr, B., Olmsted, P. D., MacKintosh, F. C. & Schmidt, C. F. Microscopic viscoelasticity: shear moduli of soft materials determined from thermal fluctuations. *Physical review letters* **79**, 3286-3289 (1997).
14 Gardel, M. L. *et al.* Elastic behavior of cross-linked and bundled actin networks. *Science* **304**, 1301 (2004).
15 Mizuno, D., Tardin, C., Schmidt, C. F. & MacKintosh, F. C. Nonequilibrium mechanics of active cytoskeletal networks. *Science* **315**, 370 (2007).
16 Rosenbluth, M. J., Crow, A., Shaevitz, J. W. & Fletcher, D. A. Slow stress propagation in adherent cells. *Biophysical journal* **95**, 6052-6059 (2008).
17 Charras, G. T., Mitchison, T. J. & Mahadevan, L. Animal cell hydraulics. *Journal of Cell Science* **122**, 3233 (2009).
18 Zicha, D. *et al.* Rapid actin transport during cell protrusion. *Science* **300**, 142-145 (2003).
19 Charras, G. T., Coughlin, M., Mitchison, T. J. & Mahadevan, L. Life and times of a cellular bleb. *Biophysical journal* **94**, 1836-1853 (2008).
20 Pollard, T. D. & Borisy, G. G. Cellular motility driven by assembly and disassembly of actin filaments. *Cell* **112**, 453-465 (2003).
21 Biot, M. A. General theory of three-dimensional consolidation. *Journal of applied physics* **12**, 155 (1941).
22 De Gennes, P. G. Dynamics of entangled polymer solutions (I&II). *Macromolecules* **9**, 587-598 (1976).

23 Mitchison, T. J., Charras, G. T. & Mahadevan, L. 215-223 (Elsevier).
24 Dembo, M. & Harlow, F. Cell motion, contractile networks, and the physics of interpenetrating reactive flow. *Biophysical journal* **50**, 109-121 (1986).
25 Hu, Y., Zhao, X., Vlassak, J. J. & Suo, Z. Using indentation to characterize the poroelasticity of gels. *Applied Physics Letters* **96**, 121904 (2010).
26 Chan, E. P., Hu, Y., Johnson, P. M., Suo, Z. & Stafford, C. M. Spherical indentation testing of poroelastic relaxations in thin hydrogel layers. *Soft Matter* **8**, 1492-1498 (2012).
27 Kalcioglu, Z. I., Mahmoodian, R., Hu, Y., Suo, Z. & Van Vliet, K. J. From macro-to microscale poroelastic characterization of polymeric hydrogels via indentation. *Soft Matter* (2012).
28 Ibata, K., Takimoto, S., Morisaku, T., Miyawaki, A. & Yasui, M. Analysis of Aquaporin-Mediated Diffusional Water Permeability by Coherent Anti-Stokes Raman Scattering Microscopy. *Biophysical journal* **101**, 2277-2283 (2011).
29 Hoffmann, E. K., Lambert, I. H. & Pedersen, S. F. Physiology of cell volume regulation in vertebrates. *Physiological reviews* **89**, 193 (2009).
30 Zhou, E. H. *et al.* Universal behavior of the osmotically compressed cell and its analogy to the colloidal glass transition. *Proceedings of the National Academy of Sciences* **106**, 10632 (2009).
31 Derfus, A. M., Chan, W. C. W. & Bhatia, S. N. Intracellular delivery of quantum dots for live cell labeling and organelle tracking. *Advanced Materials* **16**, 961-966 (2004).
32 Swaminathan, R., Bicknese, S., Periasamy, N. & Verkman, A. S. Cytoplasmic viscosity near the cell plasma membrane. *Biophysical journal* **71**, 1140-1151 (1996).
33 Kao, H. P., Abney, J. R. & Verkman, A. S. Determinants of the translational mobility of a small solute in cell cytoplasm. *The Journal of cell biology* **120**, 175-184 (1993).
34 Phillips, R. J. A hydrodynamic model for hindered diffusion of proteins and micelles in hydrogels. *Biophysical Journal* **79**, 3350 (2000).
35 Rotsch, C. & Radmacher, M. Drug-induced changes of cytoskeletal structure and mechanics in fibroblasts: an atomic force microscopy study. *Biophysical journal* **78**, 520-535 (2000).
36 Moulding, D. A. *et al.* Unregulated actin polymerization by WASp causes defects of mitosis and cytokinesis in X-linked neutropenia. *The Journal of experimental medicine* **204**, 2213 (2007).
37 Low, S. H., Mukhina, S., Srinivas, V., Ng, C. Z. & Murata-Hori, M. Domain analysis of α-actinin reveals new aspects of its association with F-actin during cytokinesis. *Experimental cell research* **316**, 1925-1934 (2010).
38 Shu, H. B. & Joshi, H. C. Gamma-tubulin can both nucleate microtubule assembly and self-assemble into novel tubular structures in mammalian cells. *The Journal of cell biology*, 1137-1147 (1995).
39 Werner, N. S. *et al.* Epidermolysis bullosa simplex-type mutations alter the dynamics of the keratin cytoskeleton and reveal a contribution of actin to the transport of keratin subunits. *Molecular biology of the cell* **15**, 990 (2004).
40 Spagnoli, C., Beyder, A., Besch, S. & Sachs, F. Atomic force microscopy analysis of cell volume regulation. *Physical Review E* **78**, 31916 (2008).
41 Albrecht-Buehler, G. & Bushnell, A. Reversible compression of cytoplasm. *Experimental cell research* **140**, 173-189 (1982).
42 Hoffman, B. D., Massiera, G., Van Citters, K. M. & Crocker, J. C. The consensus mechanics of cultured mammalian cells. *Proceedings of the National Academy of Sciences* **103**, 10259-10264 (2006).
43 Wottawah, F. *et al.* Optical rheology of biological cells. *Physical review letters* **94**, 98103 (2005).
44 Darling, E. M., Zauscher, S. & Guilak, F. Viscoelastic properties of zonal articular chondrocytes measured by atomic force microscopy. *Osteoarthritis and Cartilage* **14**, 571-579 (2006).
45 Moreno-Flores, S., Benitez, R., Vivanco, M. M. & Toca-Herrera, J. L. Stress relaxation and creep on living cells with the atomic force microscope: a means to calculate elastic moduli and viscosities of cell components. *Nanotechnology* **21**, 445101 (2010).

46 Avril, S., Schneider, F., Boissier, C. & Li, Z. Y. In vivo velocity vector imaging and time-resolved strain rate measurements in the wall of blood vessels using MRI. *Journal of biomechanics* **44**, 979-983, doi:10.1016/j.jbiomech.2010.12.010 (2011).
47 Li, P. *et al.* Assessment of strain and strain rate in embryonic chick heart in vivo using tissue Doppler optical coherence tomography. *Physics in medicine and biology* **56**, 7081 (2011).
48 Perlman, C. E. & Bhattacharya, J. Alveolar expansion imaged by optical sectioning microscopy. *Journal of applied physiology* **103**, 1037-1044 (2007).
49 Van Citters, K. M., Hoffman, B. D., Massiera, G. & Crocker, J. C. The role of F-actin and myosin in epithelial cell rheology. *Biophysical journal* **91**, 3946-3956 (2006).
50 Trepat, X. *et al.* Universal physical responses to stretch in the living cell. *Nature* **447**, 592-595 (2007).
51 Mukhina, S., Wang, Y. & Murata-Hori, M. [alpha]-Actinin Is Required for Tightly Regulated Remodeling of the Actin Cortical Network during Cytokinesis. *Developmental cell* **13**, 554-565 (2007).
52 Charras, G. & Paluch, E. Blebs lead the way: how to migrate without lamellipodia. *Nature Reviews Molecular Cell Biology* **9**, 730-736 (2008).
53 Stewart, M. P. *et al.* Hydrostatic pressure and the actomyosin cortex drive mitotic cell rounding. *Nature* **469**, 226-230 (2011).
54 DiDonna, B. & Levine, A. J. Unfolding cross-linkers as rheology regulators in F-actin networks. *Physical Review E* **75**, 041909 (2007).
55 Hoffman, B. D., Massiera, G. & Crocker, J. C. Fragility and mechanosensing in a thermalized cytoskeleton model with forced protein unfolding. *Physical Review E* **76**, 051906 (2007).
56 Luby-Phelps, K., Castle, P. E., Taylor, D. L. & Lanni, F. Hindered diffusion of inert tracer particles in the cytoplasm of mouse 3T3 cells. *Proceedings of the National Academy of Sciences* **84**, 4910 (1987).
57 Dix, J. A. & Verkman, A. S. Crowding effects on diffusion in solutions and cells. *Annu. Rev. Biophys.* **37**, 247-263 (2008).
58 Ando, T. & Skolnick, J. Crowding and hydrodynamic interactions likely dominate in vivo macromolecular motion. *Proceedings of the National Academy of Sciences* **107**, 18457-18462 (2010).
59 Gittes, F., Mickey, B., Nettleton, J. & Howard, J. Flexural rigidity of microtubules and actin filaments measured from thermal fluctuations in shape. *The Journal of cell biology* **120**, 923 (1993).

FIGURE LEGENDS:

FIGURE 1 Experimental setup. (A) Schematic diagram of the experiment. (A-I) The AFM cantilever is lowered towards the cell surface with a high approach velocity $V_{approach}$ ~30 μm.s^{-1}. (A-II) Upon contacting the cell surface, the cantilever bends and the bead starts indenting the cytoplasm. Once the target force F_M is reached, the movement of the piezoelectric ceramic is stopped at Z_M. The bending of the cantilever reaches its maximum. This rapid force application causes a sudden increase in the local stress and pressure. (A-III) and (A-IV) Over time the cytosol in the compressed area redistributes inside the cell and the pore pressure dissipates. Strain resulting from the local application of force propagates through the elastic meshwork and at equilibrium, the applied force is entirely balanced by cellular elasticity. Indentation (I-II) allows the estimation of elastic properties and relaxation (III-IV) allows for estimation of the time-dependent mechanical properties. In all panels, the red line shows the light path of the laser reflected on the cantilever, red arrows show the change in direction of the laser beam, black arrows show the direction of bending of the cantilever, and the small dots represent the propagation of strain within the cell. (B) (I) Temporal evolution of the indentation depth (black) and measured force (grey) in response to AFM microindentation normalized to values when target force is reached. Inset: approach phase from which the elasticity is calculated (grey curve). The total approach lasts ~35 ms. (II) The first 0.5 s of experimental force-relaxation curves were fitted with the poroelastic model (black line). Inset: percentage error defined as $|F_{AFM} - F_{fit}|/F_{AFM}$. (C) Z-x confocal image of a HeLa cell expressing PH-PLCδ1-GFP (a membrane marker) corresponding to phases (I) and (IV) of the

experiment described in A. The fluorescent bead attached to the cantilever is shown in blue and the cell membrane is shown in green. Scale bar =10 μm. (D) (I) Population averaged force-relaxation curves for HeLa cells (green) and MDCK cells (blue) for target indentation depths of 1.45μm for HeLa cells and 1.75μm for MDCK cells. Curves are averages of n=5 HeLa cells and n=20 MDCK cells. The grey shaded area around the average relaxation curves represents the standard deviation of the data. (II) Population averaged force-relaxation curves for HeLa cells (green) and MDCK cells (blue) from D-I plotted in a log-log scale. For both cell types, experimental force-relaxation was fitted with poroelastic (black solid line) and power law relaxations (grey solid line).

FIGURE 2 Poroelastic and elastic properties change in response to changes in cell volume. In all graphs, error bars indicate the standard deviation and, in graphs B and C, asterisks indicate significant changes ($p<0.01$ compared to control). N indicates the total number of measurements and n indicates the number of cells. In hypoosmotic shock experiments, cells were incubated with NPPB and DCPIB (N+D on the graph), inhibitors of regulatory volume decrease. (A) Cell volume change over time in response to changes in extracellular osmolarity. The volume was normalized to the initial cell volume at t=0 s. The arrow indicates the time of addition of osmolytes. (B) Effect of osmotic treatments on the elasticity E (squares) and poroelastic diffusion constant D_p (circles) in HeLa cells. (C) Effect of osmotic treatments on the elasticity E (squares) and poroelastic diffusion constant D_p (circles) in MDCK cells. (D) D_p and E plotted as a function of the normalised volumetric pore size $\psi \sim (V/V_0)^{1/3}$ in log-log plots for MDCK cells (black squares and circles) and HeLa cells (grey squares and circles). Straight lines were fitted to the experimental data points weighted by the number of measurements to reveal the scaling of D_p and E with changes in volumetric pore size (grey lines for HeLa cells, $E \sim \psi^{-1.6}$ and $D_p \sim \psi^{2.9}$ and black lines for MDCK cells, $E \sim \psi^{-5.9}$ and $D_p \sim \psi^{1.9}$).

FIGURE 3 Changes in cell volume change cytoplasmic pore size. (A) Movement of PEG-passivated quantum dots microinjected into HeLa cells in isoosmotic conditions (I) and in hyperosmotic conditions (II). Both images are a projection of 120 frames totalling 18 s (Supplementary movie I). In isoosmotic conditions, quantum dots moved freely and the time-projection appeared blurry (I); whereas in hyperosmotic conditions, quantum dots were immobile and the time-projected image allowed individual quantum dots to be identified (II). Images A-I and II are single confocal sections. In (B) and (C), dashed lines indicate loss of fluorescence due to imaging in a region outside of the zone where fluorescence recovery after photobleaching (FRAP) was measured, solid lines indicate fluorescence recovery after photobleaching and are the average of N measurements and error bars indicate the standard deviation for each time point. The greyed area indicates the duration of photobleaching. (B) FRAP of CMFDA (a fluorescein analog) in isoosmotic (black, N=19 measurements on n=7 cells) and hyperosmotic conditions (grey, N=20 measurements on n=5 cells). In both conditions, fluorescence recovered after photobleaching but the rate of recovery was decreased significantly in hyperosmotic conditions. (C) FRAP of EGFP-10x (a GFP decamer) in isoosmotic (black, N=17 measurements on n=6 cells) and hypoosmotic conditions (grey, N=23 measurements on n=7 cells). The rate of recovery was increased significantly in hypoosmotic conditions. (D) Schematic representation of the cytoplasm (I) The cytoskeleton and macromolecular crowding participate in setting the hydraulic pore size through which water can diffuse. The length-scales involved in setting cellular rheology are the average filament diameter b, the size a of particles in the cytosol, the hydraulic pore size ξ, and the entanglement length λ of the cytoskeleton. (II) Reduction in cell volume causes a decrease in cytoskeletal mesh size λ and an increase in crowding which combined lead to a decrease in hydraulic pore size ξ.

FIGURE 4 The F-actin cytoskeleton is the main biological determinant of cellular poroelastic properties. (A) Effect of F-actin depolymerisation (Latrunculin treatment), F-actin overpolymerisation (overexpression of CA-WASp), and myosin inhibition (blebbistatin treatment) on the poroelastic diffusion constant D_p. (B) Effect of F-actin depolymerisation, F-actin overpolymerisation, and myosin inhibition on the cellular elasticity E. In A and B, asterisks indicate significant changes ($p<0.01$). N is the total number of measurements and n the number of cells examined. (C) Ectopic polymerization of F-actin due to CA-WASp. HeLa cells were transduced with a lentivirus encoding GFP-CA-WASp (in green) and stained for F-actin with Rhodamine-Phalloidin (in red). Cells expressing high levels of CA-WASp (green, I) had more cytoplasmic F-actin (red, II, green arrow) than cells expressing no CA-WASp (II, white arrow). (III) zx profile of the cells shown in (I) and (II) taken along the dashed line. Cells

expressing CA-WASp displayed more intense cytoplasmic F-actin staining (green arrow) than control cells (white arrow). Cortical actin fluorescence levels appeared unchanged. Nuclei are shown in blue. Images I and II are single confocal sections. Scale bars =10 μm.

Figure 1

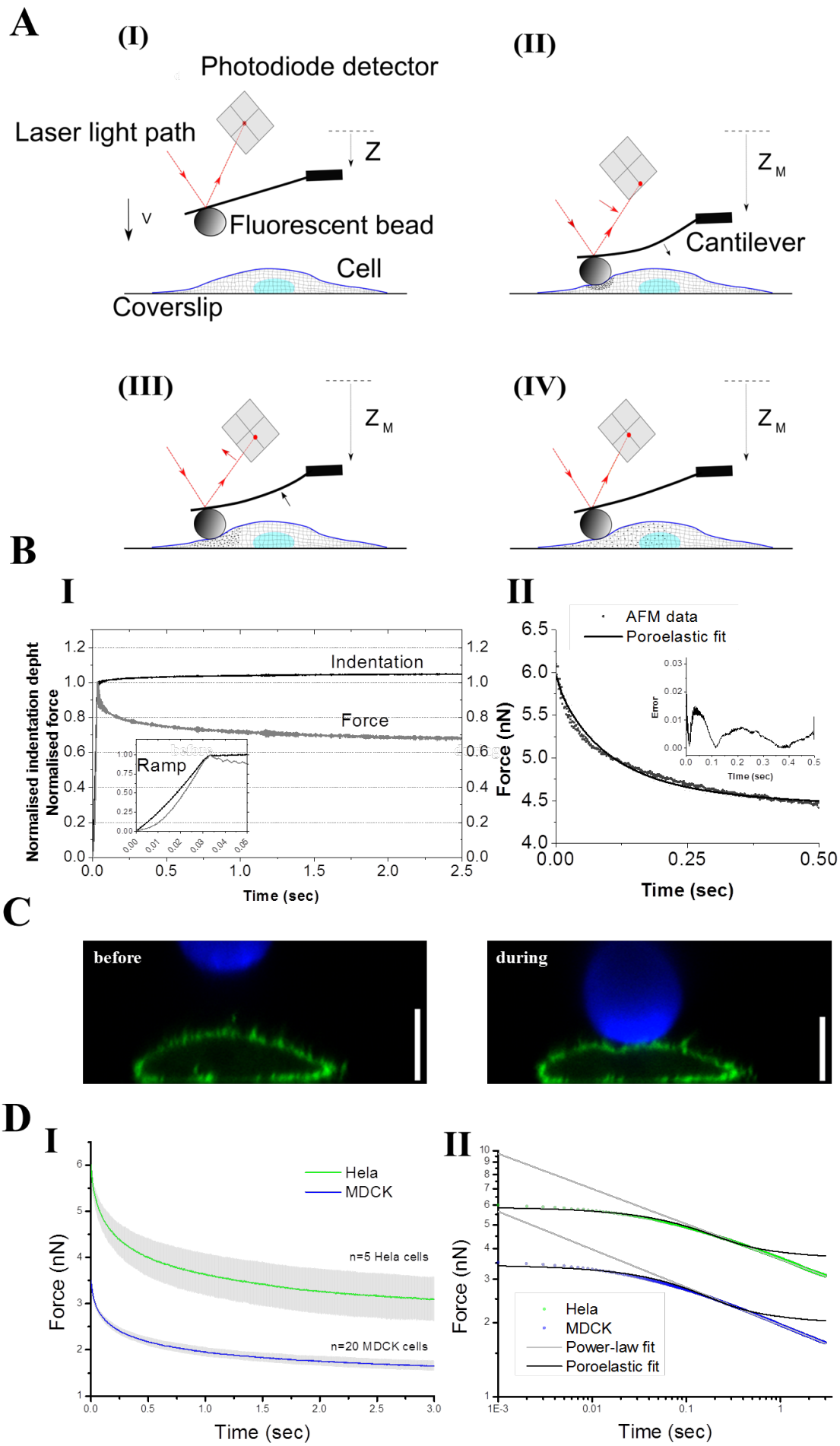
A
(I)
Photodiode detector
Laser light path
Z
V
Fluorescent bead
Cell
Coverslip
(II)
Z M
Cantilever
(III)
Z M
(IV)
Z M
B
I
Normalised indentation depht
Normalised force
Indentation
Force
Ramp
Time (sec)
II
AFM data
Poroelastic fit
Error
Time (sec)
Force (nN)
Time (sec)
C
before
during
D
I
Hela
MDCK
n=5 Hela cells
n=20 MDCK cells
Force (nN)
Time (sec)
II
Hela
MDCK
Power-law fit
Poroelastic fit
Force (nN)
Time (sec)

Figure 2

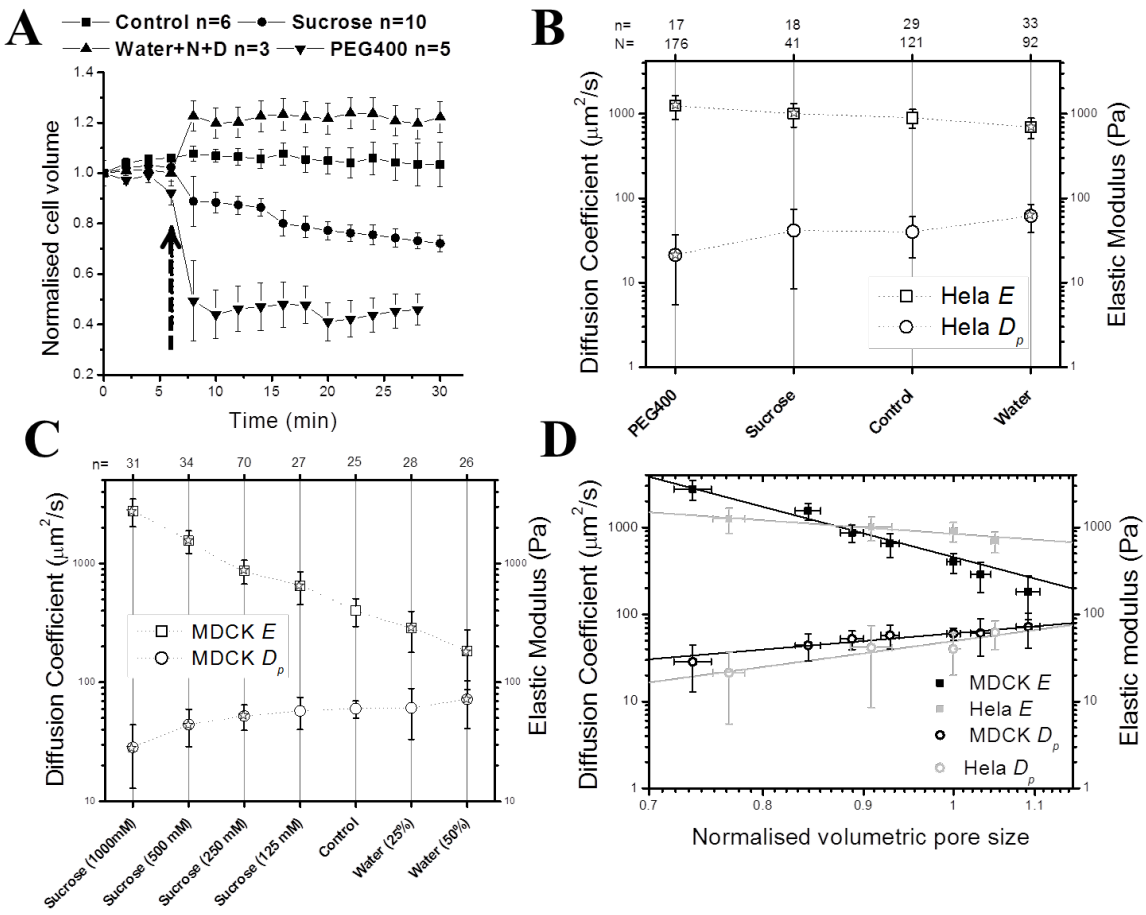
A
Control n=6
Sucrose n=10
Water+N+D n=3
PEG400 n=5
Normalised cell volume
Time (min)
B
n= 17 18 29 33
N= 176 41 121 92
Diffusion Coefficient (μm²/s)
Elastic Modulus (Pa)
Hela E
Hela Dp
PEG400
Sucrose
Control
Water
C
n= 31 34 70 27 25 28 26
MDCK E
MDCK Dp
Sucrose (1000mM)
Sucrose (500 mM)
Sucrose (250 mM)
Sucrose (125 mM)
Control
Water (25%)
Water (50%)
D
MDCK E
Hela E
MDCK Dp
Hela Dp
Normalised volumetric pore size
Elastic modulus (Pa)

Figure 3

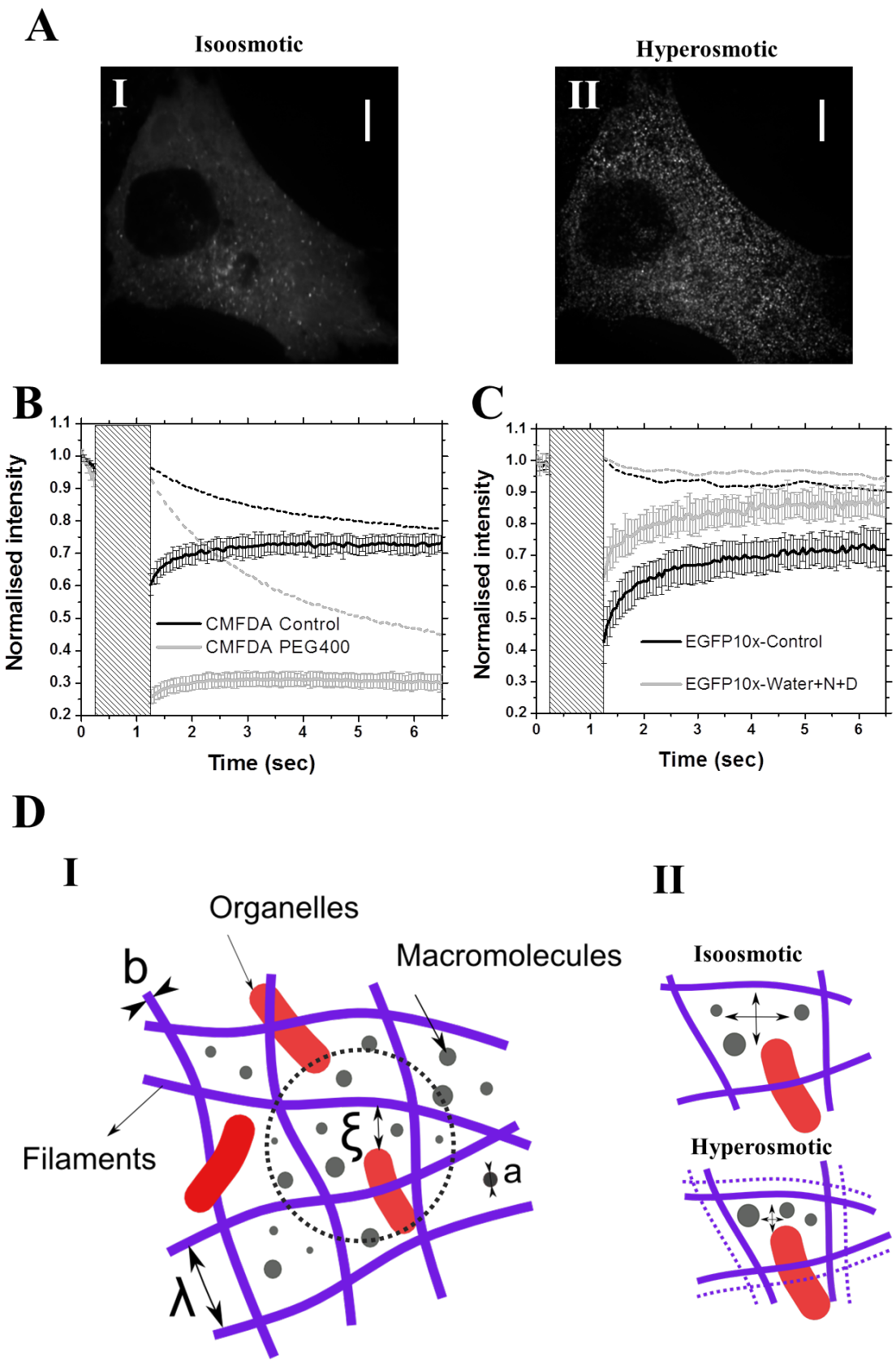
A
Isoosmotic
Hyperosmotic
I
II
B
Normalised intensity
Time (sec)
CMFDA Control
CMFDA PEG400
C
Normalised intensity
Time (sec)
EGFP10x-Control
EGFP10x-Water+N+D
D
I
Organelles
Macromolecules
b
Filaments
ξ
a
λ
II
Isoosmotic
Hyperosmotic

Figure 4

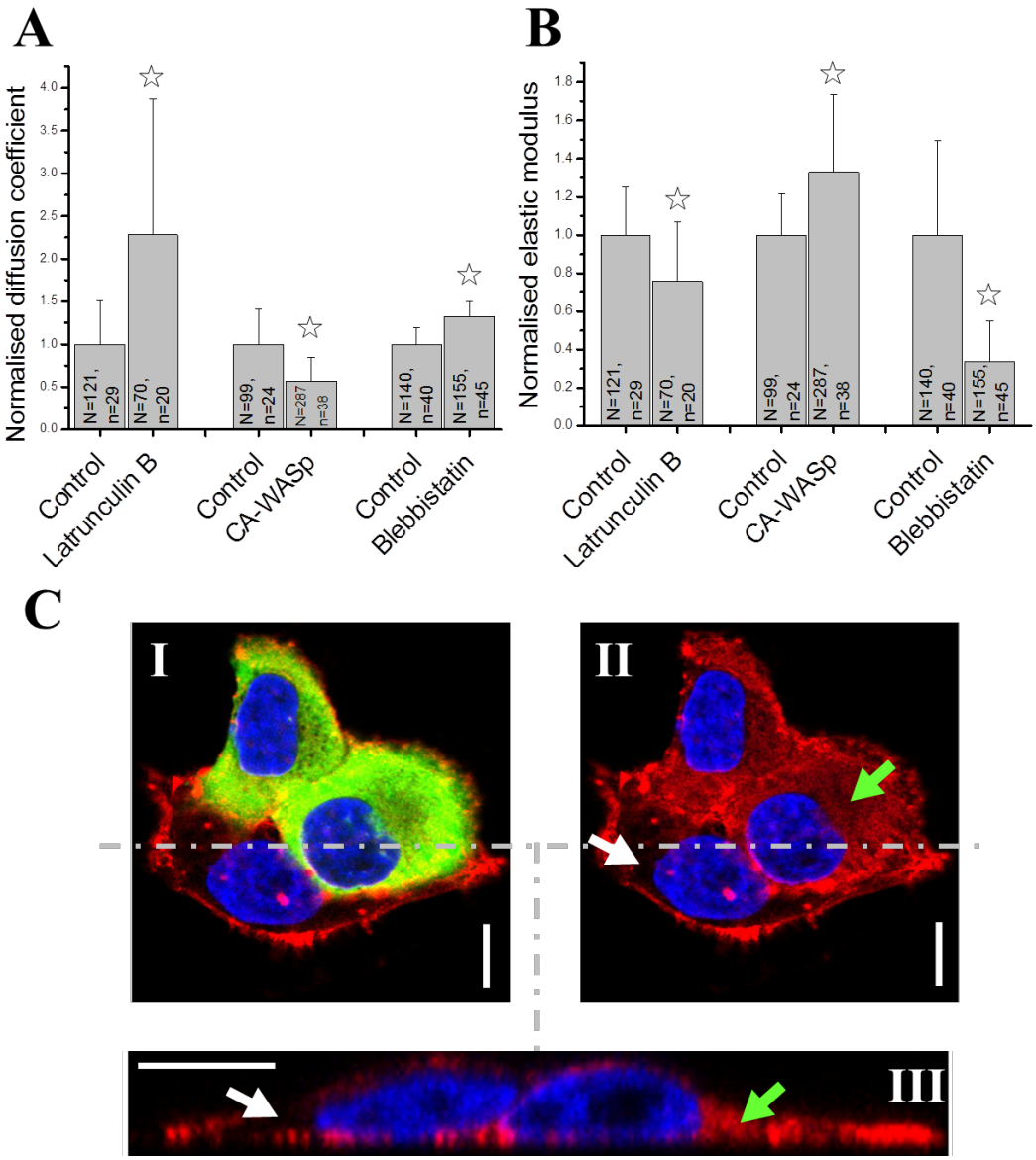
A
Normalised diffusion coefficient
4.0
3.5
3.0
2.5
2.0
1.5
1.0
0.5
0.0
N=121, n=29
N=70, n=20
N=99, n=24
N=287 n=38
N=140, n=40
N=155, n=45
Control
Latrunculin B
Control
CA-WASp
Control
Blebbistatin
B
Normalised elastic modulus
1.8
1.6
1.4
1.2
1.0
0.8
0.6
0.4
0.2
0.0
N=121, n=29
N=70, n=20
N=99, n=24
N=287, n=38
N=140, n=40
N=155, n=45
Control
Latrunculin B
Control
CA-WASp
Control
Blebbistatin
C
I
II
III